SEMARAK ILMU PUBLISHING

CFD Letters

Journal homepage:
https://semarakilmu.com.my/journals/index.php/CFD_Letters/index
ISSN: 2180-1363

Aerodynamic Drag Reduction using a Conduit in the Ahmed Body

Amine Agriss[1,*], Mohamed Agouzoul[1], Abdeslem Ettaouil[1]

[1] ERG2(ME), Mohammed V University in Rabat, Mohammadia School of Engineering, Avenue Ibn Sina, P.O. Box 765-Agdal, Rabat, Morocco

ARTICLE INFO

Article history:
Received 1 March 2024
Received in revised form 21 May 2024
Accepted 17 August 2024
Available online 30 November 2024

Keywords:
Drag; Ahmed body; aerodynamics; conduit; numerical model; turbulent flow

ABSTRACT

In this study, the focal challenge is reducing drag around the Ahmed body, a critical concern in aerodynamics. The approach involves perforating a rectangular conduit inside the body, redirecting part of the airflow from the front to the rear end to minimize drag. Using Ansys Fluent CFD software and the SST $k-\omega$ turbulence model, a numerical model for turbulent flow around a 3D body has been developed. Through a series of numerical simulations, variations in the conduit's position relative to the lowest slanted edge of the body have been explored. At the optimal position with the lowest drag, an examination has been conducted on the narrowing of the conduit outlet dimensions. Results indicate that, with a suitable conduit position and an appropriate exit narrowing, a decrease in drag of up to 3% could be achieved. Ongoing work involves the examination of the conduit's tilt at the outlet to determine the optimal arrangement for further drag reduction. This research offers practical insights for drag reduction and contributes to the broader field of aerodynamics.

1. Introduction

To achieve a high automotive performance, reducing the aerodynamic drag is of great benefit in future vehicle designs. In fact, at least 21% of the entire fuel consumption of a vehicle, moving at 105 km.h^{-1}, is due to aerodynamic drag, which rises quadratically with relative vehicle velocity [1]. A division is made in the aerodynamic drag, separating it into pressure and friction components. For the simplified car model called Ahmed body, the pressure drag makes up about 85% of the overall drag, and the body's rear end is primarily responsible for this [2]. The Ahmed body is extensively employed as a benchmark in order to represent essential flow characteristics surrounding an automobile vehicle. Ahmed *et al.,* [2] initially introduced it in 1984. Today it has become a standard for aerodynamic simulations.

With the goal of minimizing drag, various strategies have been proposed. These strategies are carried out experimentally or numerically using Computational Fluid Dynamics (CFD) software. One of these strategies is flow control, which can be either active or passive. While the first solution relies on an external power supply, the second approach operates autonomously without need for one. Even if active flow control techniques were convenient and effective, they are expensive. As a result,

* *Corresponding author.*
E-mail address: amineagriss@research.emi.ac.ma (Amine Agriss)

https://doi.org/10.37934/cfdl.17.5.2644

the employment of passive strategies, including bio–inspired designs [3], is always favored by adjusting the geometrical design [4], employing extra external features and modifying or organizing the arrangement of the devices on the simplified automobile model [5]. In addition to the Ahmed body, other simplified models, such as flat plates or aerodynamic airfoils, are utilized to evaluate drag reduction devices before real–world use [6–9].

Flow control techniques applied to the Ahmed body encompass a diverse range of strategies aimed at optimizing its aerodynamic performance. Among these strategies are passive adjustments, which involve modifying the body's geometric shape and incorporating various surface devices. Researchers have explored various methods such as integrating base cavities, installing vertical breakup plates, employing rounded edges, utilizing automatic moving deflectors, deploying flaps, incorporating connecting tunnels, and refining the body shape [10–18]. These strategies, among others, serves the common goal of optimizing airflow around the vehicle, ultimately resulting in reduced drag and improved overall efficiency. In addition to passive adjustments, active flow control strategies are crucial in optimizing aerodynamic performance. These techniques involve actively managing airflow using mechanisms such as constant microjets, unstable jets, pulsed jets, synthetic jets, periodic–forcing jets, pulsed jets with porous layers, and employing adaptable Coanda devices or side air–knife blowers [19–26]. By dynamically adjusting airflow patterns, these methods, among others, can further enhance aerodynamic efficiency, leading to reduced drag and improved vehicle performance. Extensive literature details these techniques, providing valuable insights into their effectiveness and applications in aerodynamic design and optimization.

This investigation focuses on the 25° slant Ahmed body. The C–pillar vortices, or longitudinal swirls, govern the overall arrangement of flow at the recirculation zone [27]. As a result, the flow separation zone significantly adds to drag. To address this issue and reduce drag of this model, the main idea in this study is to perforate a rectangular conduit into the body to inject a flow part at the body’s rear recirculation zone. The optimal distance, measured at the lowest slant edge, yields the smaller drag coefficient for various dimensions within this conduit. For this distance, and to speed up the flow, dimensions of conduits are reduced at the outlet. Based on the conduit’s size and exit reduction ratio, different designs are examined. The suitable configuration is found to minimize drag.

Unlike conventional active flow control methods explored by various researchers, our approach involves manipulating the flow upstream of the Ahmed body. This straightforward yet innovative method effectively diminishes drag by passively targeting the recirculation region, operating with the efficiency of active flow control but without the need for external energy input. Nevertheless, it is essential to recognize the limitations inherent in our methodology, notably in the context of our numerical simulations' scope. This research is an extension of the previous 2D investigation conducted on the same drag reduction device [4].

2. Numerical Simulation and Physical Model

2.1 Configuration Studied

The purpose of this research is to examine drag reduction by implementing a perforated rectangular conduit within the Ahmed body. A number of numerical simulations using various conduit configurations have been performed. Initially, various conduit dimensions are tested, followed by reducing exit dimensions for optimal vertical placement, resulting in lower drag coefficients. All results are compared based on drag coefficients.

The Ahmed body is employed for a variety of testing. It measures 1044 mm in length, 288 mm in height and 389 mm in width. With various slanted angles φ, the slant portion is 222 mm in length. The body is 50 mm above ground level. It’s supported by four stilts with a diameter of 30 mm each.

The purpose of these stilts is to immobilize the body during experimental testing. They contribute little to the drag force, and they are not taken into account in this study. Figure 1 displays the geometric characteristics of the 25° slant angle Ahmed body.

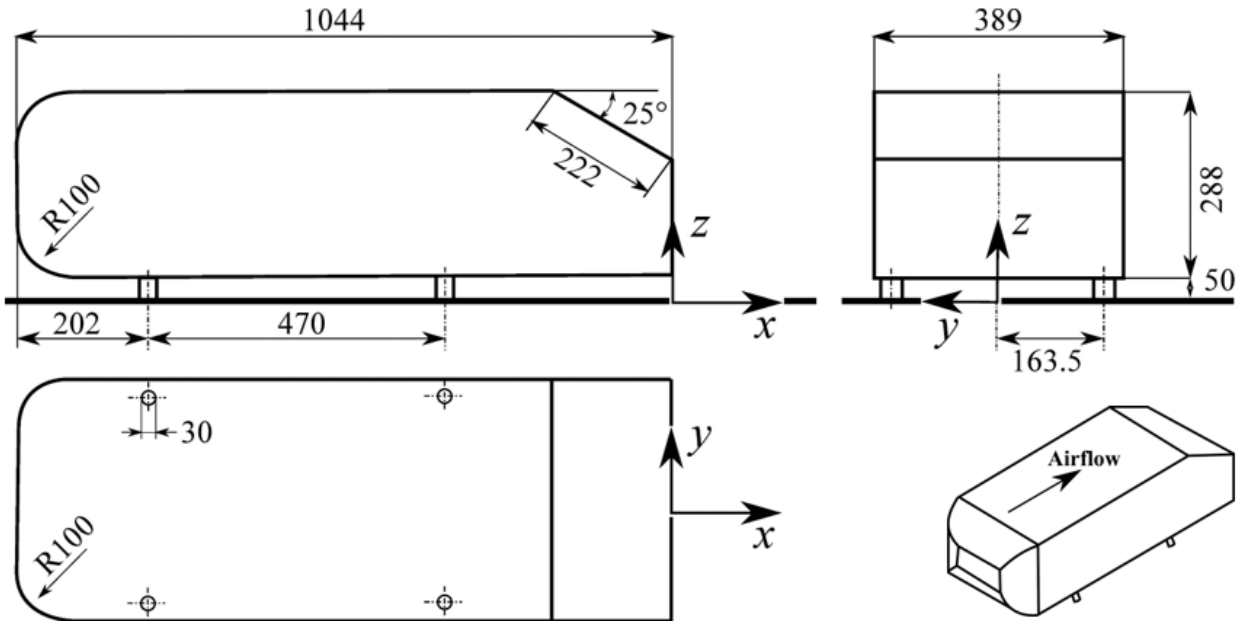

Fig. 1. Ahmed body geometry (mm)

A rectangular conduit is introduced into the body, as depicted in Figure 2. Its goal is to redirect a portion of incoming flow to the recirculation zone. *L* and *l* are the geometrical characteristics of the conduit, where *L* is its length and *l* is its width. The conduit is symmetrical with respect to the *z*–axis.

With varying conduit distances (*H*) beginning from the Ahmed body's tilted lower edge, different tests are performed for various conduit lengths (*L*) and widths (*l*).

For the position that gives lowest drag coefficients, the consequence of narrowing the conduit at the outlet by the same factor ($R = \frac{L}{L'} = \frac{l}{l'}$) is evaluated. This reduction in dimensions allows the flow acceleration at the exit of the conduit and may reduce the Ahmed body's drag coefficient.

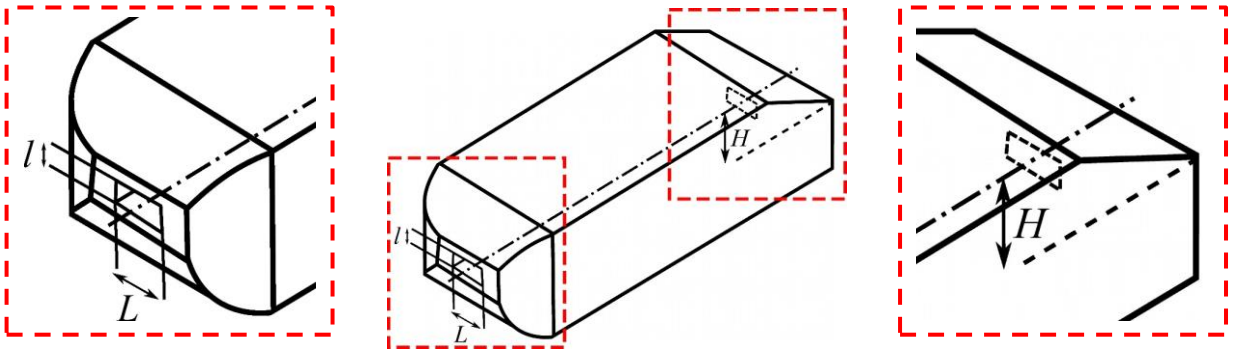

(a) (b) (c)

Fig. 2. Conduit characteristics (a) Conduit dimensions (b) Overall view (c) Conduit placement

Figure 3 shows the geometrical characteristics of the narrowed conduits. *L'* and *l'* denote the size specifications of the conduit at the exit point. Several setups are examined while varying the factor *R* each time.

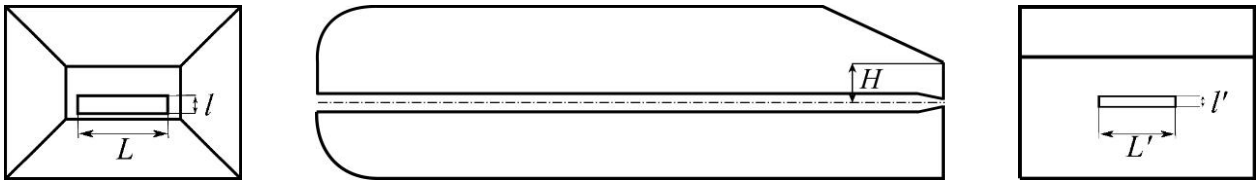

(a) (b) (c)

Fig. 3. Reducing the conduit at the outlet (a) Conduit dimensions at the inlet (b) Conduit location (c) Conduit dimensions at the exit

2.2 Governing Equations

The equations of continuity and Reynolds–Averaged Navier–Stokes govern turbulent incompressible steady flows. They are defined by:
Continuity:

$$\frac{\partial u_i}{\partial x_i} = 0 \tag{1}$$

Momentum:

$$\rho \frac{\partial \left(u_j u_i\right)}{\partial x_j} = -\frac{\partial p}{\partial x_i} + \frac{\partial}{\partial x_j}\left[\mu\left(\frac{\partial u_i}{\partial x_j}\right) - \rho\overline{u_j' u_i'}\right] \tag{2}$$

Where u_i and u_j represent the mean velocity components, ρ denotes the density, p signifies the mean pressure and μ denotes the dynamic viscosity.

$\rho\overline{u_j' u_i'}$ represents the effect of turbulence on average characteristics of fluid motion.

To close Eq. (2), Reynolds stresses must be modeled. Under the hypothesis of Boussinesq [28], which defines the turbulent viscosity μ_t, the constraints of Reynolds are defined by:

$$-\rho\overline{u_i' u_j'} = \mu_t\left(\frac{\partial \overline{u}_j}{\partial x_i} + \frac{\partial \overline{u}_i}{\partial x_j}\right) - \frac{2}{3}\rho k\delta_{ij} \quad \text{with} \quad \delta_{ij} = \begin{cases} 1 & \text{for } i = j \\ 0 & \text{for } i \neq j \end{cases} \tag{3}$$

k represents the turbulent kinetic energy.

In this work, the turbulence model employed is SST k–ω. This particular model, relying on Boussinesq approximation, is developed by Menter [29] in 1994. It is accurate for flows around bluff bodies and flows with adverse pressure gradient [30]. More details about this model are available in the literature [31].

The SST k–ω turbulence model can be applied for both low and high numbers of Reynolds. Through the utilization of a blending function to formulate the near–wall zone, wall boundary conditions switch automatically from a low–Reynolds number treatment ($y^+ \leq 30$) to a wall function treatment ($30 \leq y^+ \leq 300$) considering the mesh density. To save the computational time and to

have a numerical stability, the use of wall function treatment has proven to provide good results for low drag configurations like the Ahmed body [32, 33].

The definition of drag coefficient is as follows:

$$C_d = \frac{F_d}{\frac{1}{2}\rho U^2 A} \tag{4}$$

F_d refers to the force of drag, U represents the velocity of fluid flow, and A denotes the vehicle's frontal area as viewed from the direction of flow.

At each iteration of the numerical simulations, the components of pressure and wall shear forces, aligned with the direction of flow around the geometry, are integrated to calculate the drag force.

The definition of drag force is as follows:

$$F_d = \int p\vec{n}ds\vec{i} + \int \tau_w \vec{t}ds\vec{i} \tag{5}$$

Where the pressure p and the wall shear τ_w acts, on a differential body area ds, are pds and $\tau_w ds$.

$\vec{i}$ denotes the flow direction unit vector.

$\vec{t}$ and $\vec{n}$ denote unit vectors in directions normal and tangential to the surface with area ds.

2.3 Conditions of Simulations

This section outlines the parameters used in the numerical simulations. This work is carried out using the Ansys Fluent 17.0 program.

2.3.1 Geometry creation

Geometries are created using Ansys Design Modeler module. The overall flow domain dimensions are depicted in Figure 4. To give an appropriate air growth around the body, the blockage ratio is about 1.71%. To prevent any interference with the flow solution, boundary conditions are established sufficiently distant from the body. The body is located at $3L_c$ away from the inlet, $5L_c$ from the outlet, $1.5L_c$ from the side and $2L_c$ from the top. L_c = 1.044 m is the characteristic body's length. The body is away from the ground by 0.05 m as in experimental investigations [34]. To decrease the simulation duration, the symmetry condition is also employed.

2.3.2 Mesh generation

Meshes are created with Ansys Mesh Module. As shown in Figure 5(a), an unstructured tetrahedral mesh is used. The perspective view is also given in Figure 5(b). To obtain a precise simulation of flow within the body's boundary layer, a five–layer inflation is utilized, as illustrated in Figure 5(c).

The dimensionless mesh spacing, denoted as y^+, serves as a representation of the meshes resolution. It is an important turbulence modeling parameter that allows determining the proper size

of near domain cells. In this study, except for some small regions, $30 \leq y^{+} \leq 300$ as shown in Figure 6. In this case, the first cell size is situated within the log–law zone. Consequently, employing the wall function results in a reduction in computation time.

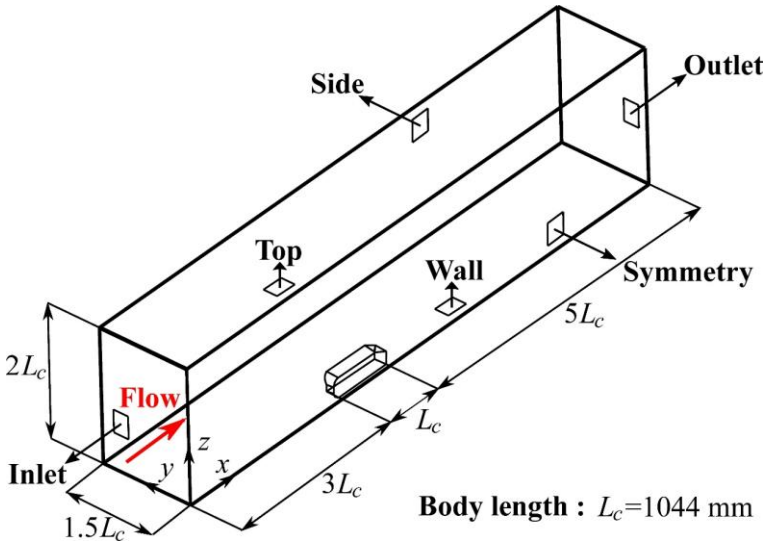

Fig. 4. Numerical flow domain

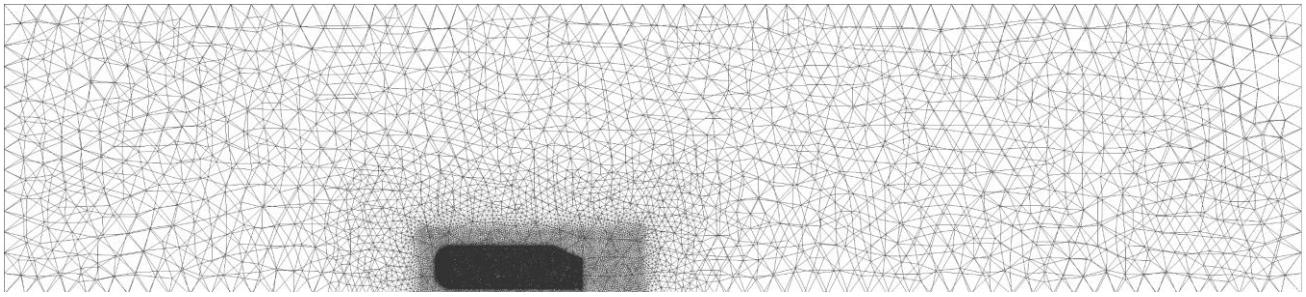

(a)

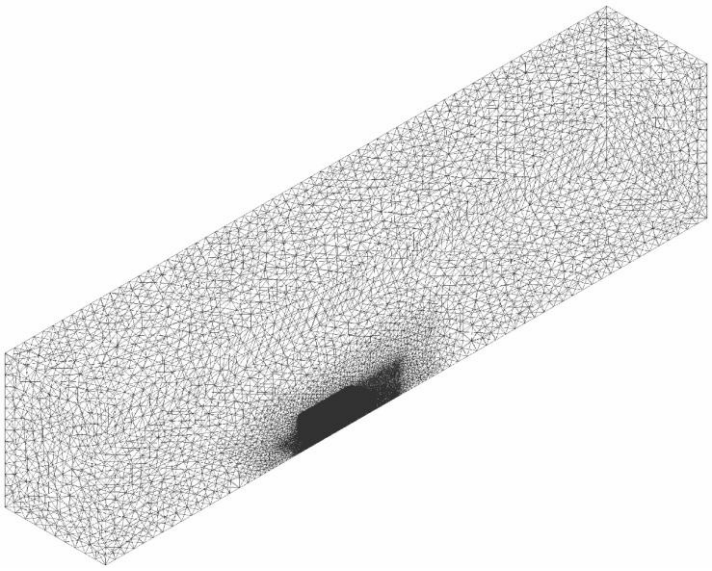

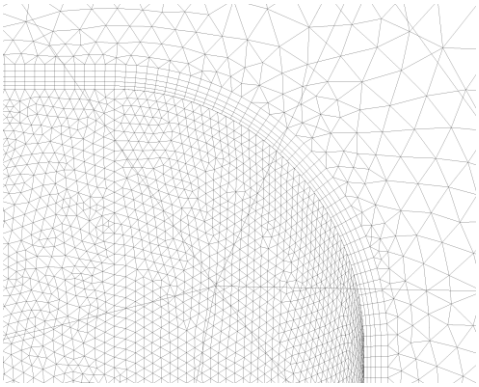

(b) (c)

Fig. 5. Mesh structure (a) In the symmetry plan (b) Perspective view (c) Details of the inflation

2.3.3 Physical model

Airflow modelling: Within this investigation, an incompressible and viscous airflow is used, characterized by a viscosity of 1.7894×10^{-5} kg.m^{-1}.s^{-1}, density of 1.225 kg.m^{-3} and velocity of 40 m/s. With respect to the body length, the Reynolds number is given as Re = 2.85×10^{6}.

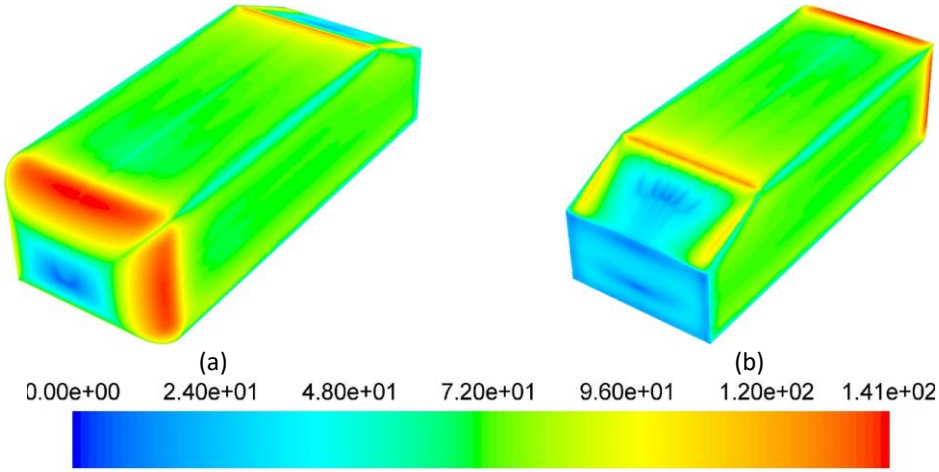

Fig. 6. y^{+} along the Ahmed body (a) Front view (b) Rear view

Airflow is solved using steady–state turbulent RANS approaches. The SST k–ω turbulence model is employed. The Pressure–Velocity Coupling Method utilizes a coupled scheme for the solution. The Green–Gauss Node–Based approach is utilized to solve gradients. The second order and the second order upwind schemes are utilized to solve pressure, momentum and turbulence equations.

Boundary conditions: Figure 7 illustrates the boundary conditions employed in numerical simulations. The Ahmed body acts as an immovable, non–slip wall. Boundary conditions for k and ω are established by taking into account a turbulent intensity at inlet of 1% and a ratio of turbulent viscosity of 10.

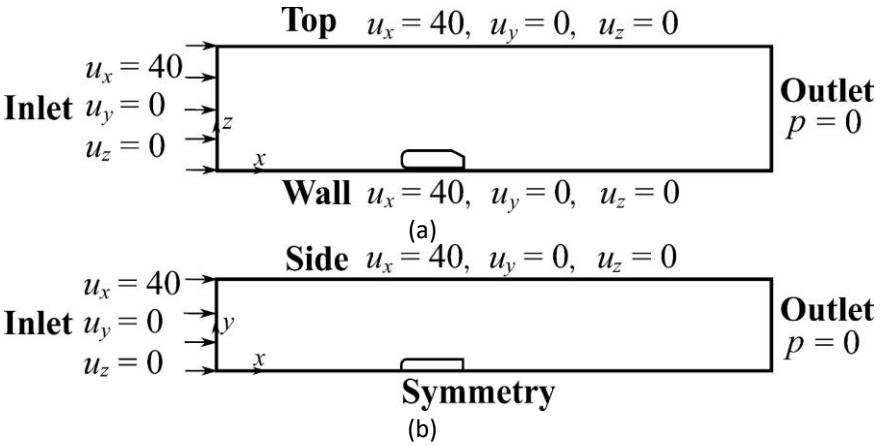

Fig. 7. Boundary conditions (a) View from the front (b) View from the top

Convergence: To ensure convergence, the residuals of continuity and velocity equations, as well as turbulence quantities, are set to 10^{-7}. The drag coefficient is additionally employed for gauging convergence. Based on Figure 8, it can be observed that upon 400 iterations, residuals of x–velocity, y–velocity, and z–velocity converge. Yet, the residual of continuity has an asymptotic value less than

10^{-4}. The calculations are then terminated upon reaching 1000 iterations. As seen in Figure 9, drag coefficient also remains constant after 400 iterations.

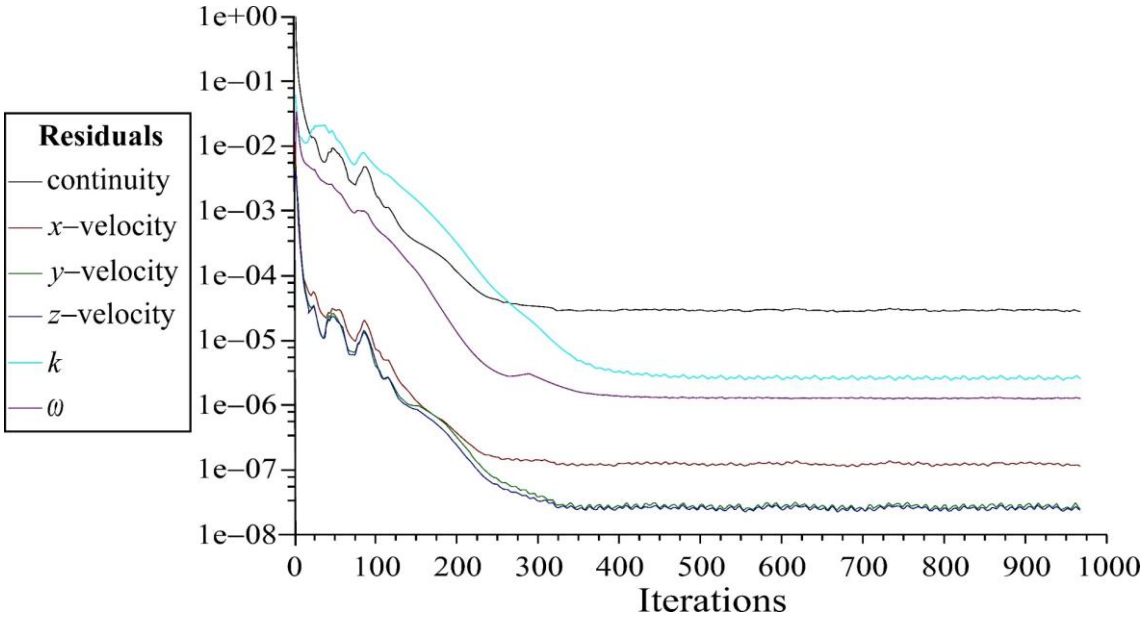

Fig. 8. Residual monitors

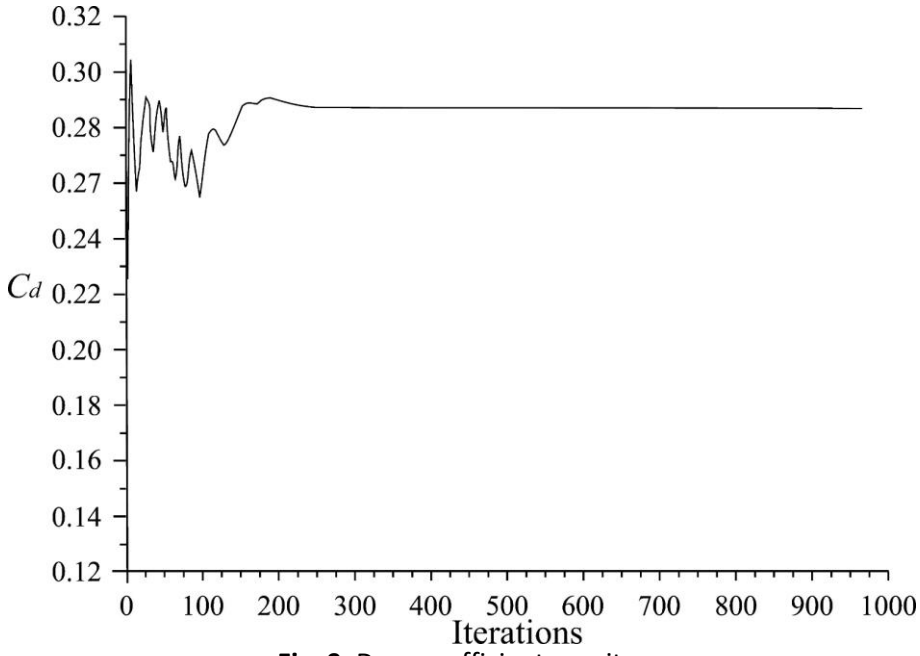

Fig. 9. Drag coefficient monitor

3. Numerical Simulation and Physical Model

All numerical outcomes are reported in this section. First, a study of the mesh influence on the numerical results. Then, a validation of the simulation results with previous results. Finally, a presentation of results allowing finding the optimal configuration reducing the most drag.

3.1 Mesh Influence Study

Examining the grid influence is essential to ensure that the findings from simulations are not affected by mesh size. Figure 10 illustrates that drag coefficient remains unaffected by variations in the grid mesh size. Hence, the grid of 1 502 900 elements is preserved to secure the precision of the upcoming simulations.

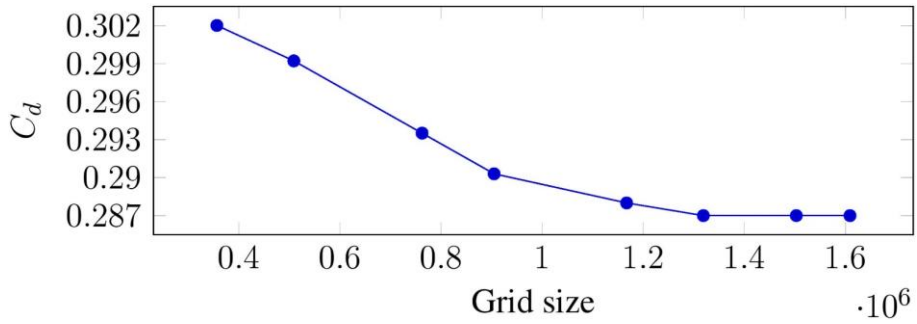

Fig. 10. Grid independence study

3.2 Validation of Numerical Model

A numerical simulation is conducted without using the device within the Ahmed body. Results are compared with findings from existing literature sources. Based on Table 1, the drag coefficient obtained from the current calculations aligns with the experimental results [2], as well as with the findings from both 2D [35] and 3D numerical simulations [36].

Table 1
Verification of drag coefficient

	Current research	3D result [36]	2D result [35]	Experiment result [2]
C_d	0.287	0.3074	0.3008	0.285

Figure 11 shows that the velocity fields, obtained in the present simulation, agree with previous numerical [20, 32] and experimental [37, 38] results.

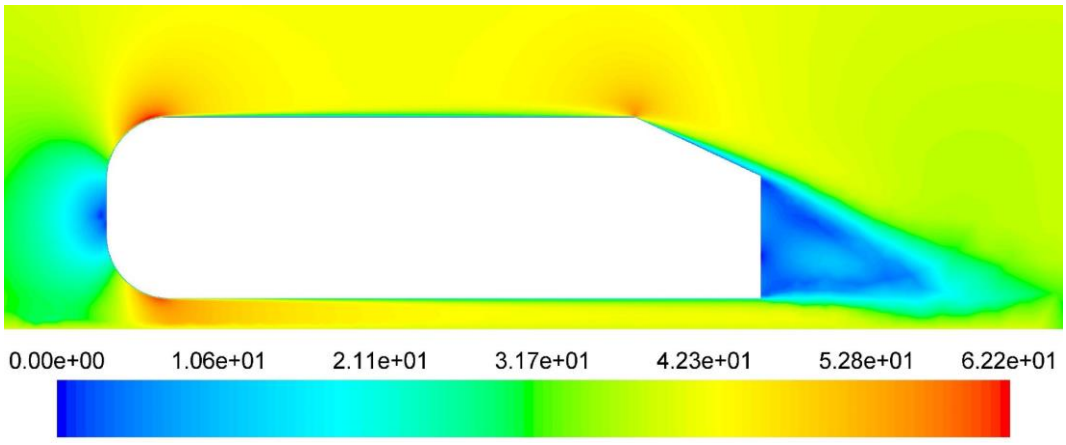

Fig. 11. Velocity contours surrounding Ahmed body ($m.s^{-1}$)

3.3 Simulations Results

Drawing upon the historical context of passive control of flow, the majority of solutions concentrate on the body's exterior surfaces, incorporating various equipment. While conducting this study, particular attention is given to the internal body's components to discover a groundbreaking solution to minimize drag. Through the implementation of a perforated conduit within the body, flow control is achieved by capitalizing on the advantages offered by the upstream flow. In addition, this new technique operates without the need for any external energy input.

Different arrangements of conduits are examined to identify which one reduces the most drag. Initially, the conduit's placement is modified by adjusting *H*, distance from the bottom slanted edge. The conduit is characterized by two parameters, its length (*L*) and its width (*l*). Several conduits with various dimensions are evaluated for each distance *H*.

In Table 2, Table 3 and Table 4, the drag coefficients of the Ahmed body with different uniform conduit setups are presented, each at varying distances *H*. To offer deeper insight into these findings, they are visually depicted in Figure 12.

Table 2
Drag coefficients for conduits placed at *H* = 0.03 m

		***L* (m)**		
		0.02	0.06	0.1
***l* (m)**	0.02	0.287	0.29	0.293
	0.04	0.289	0.299	0.301
	0.06	0.291	0.303	0.306
	Ahmed body	0.287	0.287	0.287

Table 3
Drag coefficients for conduits placed at *H* = 0.07 m

		***L* (m)**		
		0.02	0.06	0.1
***l* (m)**	0.02	0.288	0.294	0.3
	0.04	0.291	0.304	0.307
	0.06	0.2958	0.3127	0.3145
	Ahmed body	0.287	0.287	0.287

Table 4
Drag coefficients for conduits placed at *H* = 0.1 m

		***L* (m)**		
		0.02	0.06	0.1
***l* (m)**	0.02	0.291	0.301	0.307
	0.04	0.297	0.313	0.317
	0.06	0.304	0.318	0.325
	Ahmed body	0.287	0.287	0.287

Contrary to our goal of minimizing drag, the coefficients exceed the standard drag coefficient (i.e., in the absence of conduits) for every evaluated conduit configuration. Meanwhile, the examination of narrowed conduit setups may provide valuable insights into mitigating drag. Specifically, the narrowing of conduit dimensions at the exit may accelerate flow, potentially providing a means to achieve our goal of drag reduction.

H = 0.03 m is identified to be the optimal position because it allows lower drag coefficients among all other distances. This distance will be conserved in the next simulations. In these simulations, the

conduit exit is shortened without inclination. The conduit exit has new shortened dimensions *L'* and *l'*. The reduction ratio link between conduit dimensions at the inlet and exit ($R = \frac{L}{L'} = \frac{l}{l'}$).

To examine the effect of different conduit sizes, a range of reduction ratios for the conduit's exit are tested while maintaining the conduit at a distance of *H* = 0.03 m.

Table 5, Table 6 and Table 7 outline the drag coefficients of Ahmed body for different narrowed conduit configurations across various reduction factors. To elucidate their progression further, these results are visually represented in Figure 13.

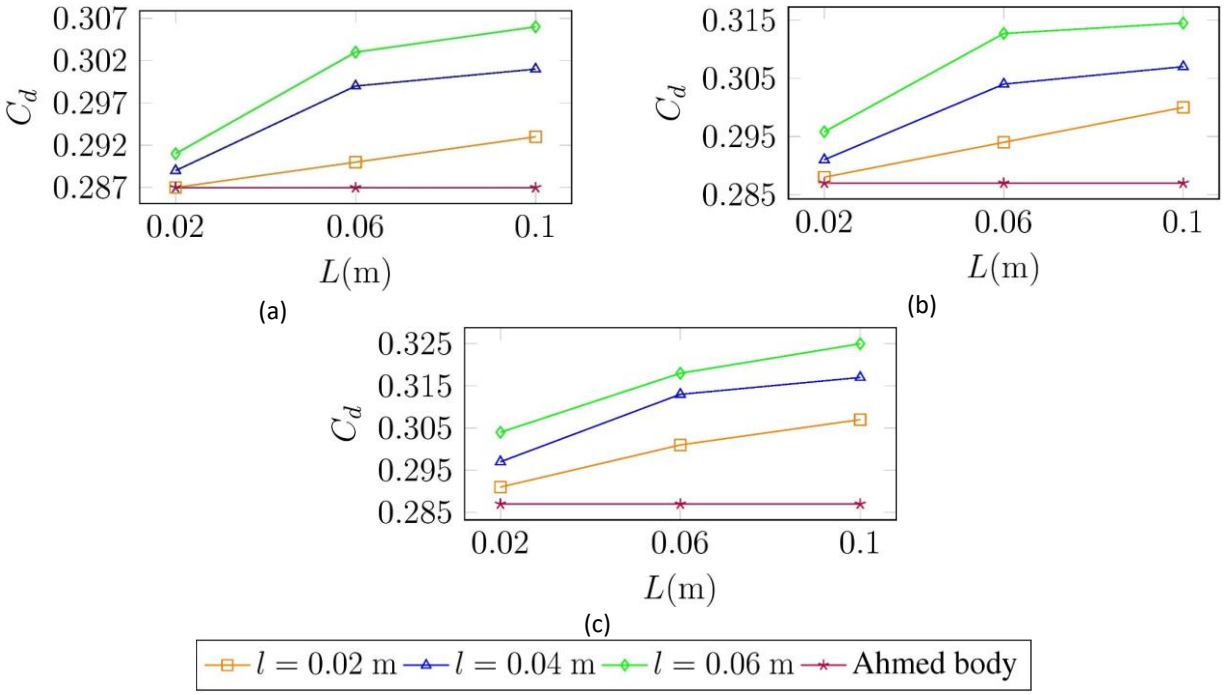

Fig. 12. Drag coefficients of various conduit layouts set at different positions from the lowest slanted edge (a) *H* = 0.03 m (b) *H* = 0.07 m (c) *H* = 0.1 m

Table 5
Drag coefficients for conduits with a reduction ratio *R* = 2

		***L* (m)**		
		0.02	0.06	0.1
***l* (m)**	0.02	0.286	0.282	0.288
	0.04	0.286	0.288	0.292
	0.06	0.287	0.291	0.297
	Ahmed body	0.287	0.287	0.287

Table 6
Drag coefficients for conduits with a reduction ratio *R* = 4

		***L* (m)**		
		0.02	0.06	0.1
***l* (m)**	0.02	0.285	0.2785	0.285
	0.04	0.2855	0.283	0.289
	0.06	0.2855	0.286	0.2895
	Ahmed body	0.287	0.287	0.287

Table 7
Drag coefficients for conduits with a reduction ratio R = 6

		***L* (m)**		
		0.02	0.06	0.1
***l* (m)**	0.02	0.2865	0.2863	0.2864
	0.04	0.2863	0.2858	0.286
	0.06	0.2865	0.2868	0.2873
	Ahmed body	0.287	0.287	0.287

All reduction ratios found give drag coefficients lower than drag coefficients of the same conduit configurations without output reduction. This fact confirms that the reduction in dimensions at the exit accelerates the flow and has a beneficial impact on the reduction of drag.

The ratio R = 4 is identified as the most optimal one. It enables drag reduction, particularly for a conduit measuring 0.06 m in length and 0.02 m in width, resulting in a drag decrease up to 3%.

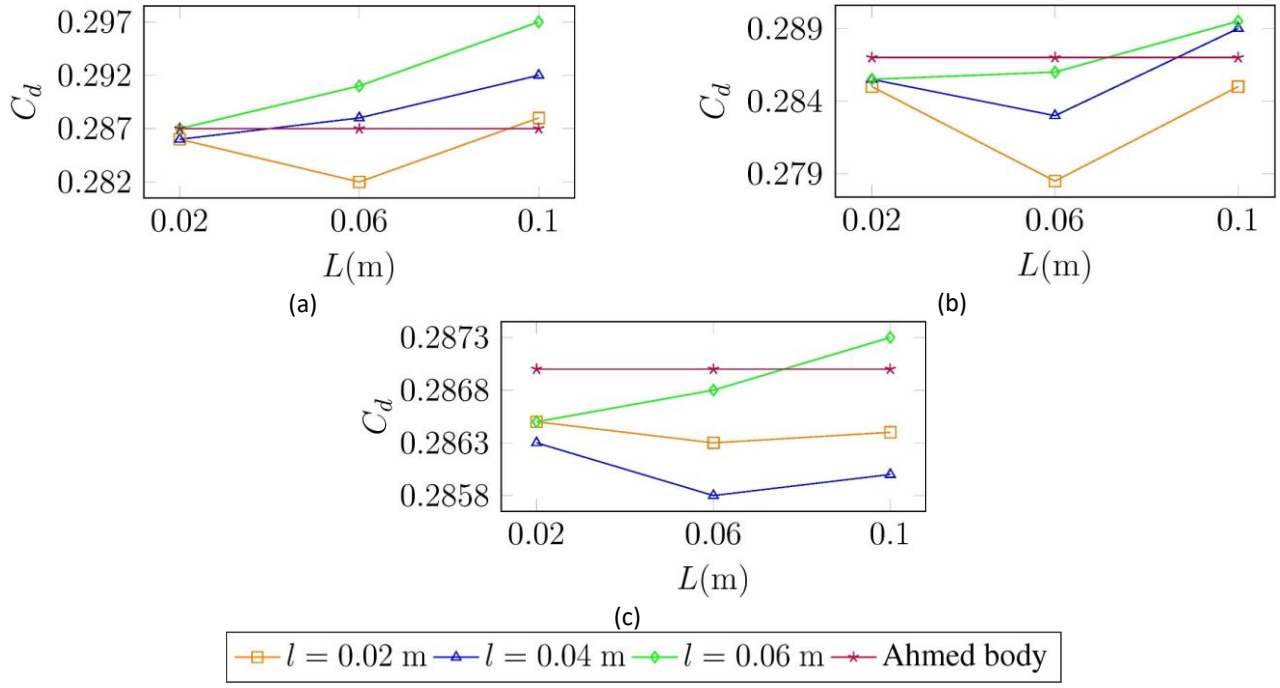

Fig. 13. Effect of varying exit reduction ratios of conduits on drag coefficient (a) R = 2 (b) R = 4 (c) R = 6

Streamlines of the specific configurations are compared with the Ahmed body's streamlines with absence of conduits. Figure 14 shows a comparison between the streamlines of the standard Ahmed body (Figure 14 (a)), the configuration that gives the highest drag coefficient (the conduit measuring L = 0.1 m and l = 0.06 m, positioned at H = 0.1 m from lowest slant edge) (Figure 14 (b)) and the configuration that gives the maximum drag reduction (Figure 14 (c)).

In conduits with uniform dimensions, especially in unfavorable cases, drag coefficients increase compared to the reference value. This is attributed to the maintained uniform velocity of airflow upstream of the body. Since drag is proportional to the square of internal velocity, reducing conduit dimensions becomes essential, leading to decreased flow velocity and, consequently, reduced drag. The reduced dimensions also result in an outlet flow acceleration, contributing to a potential reduction in the recirculation zone and, thereby, minimizing drag. This phenomenon is notably observed in favorable cases.

Figure 15 presents a comparison of the contours of velocity, of the same specific setups, at the plane z = 0.1 m. For the configuration with the highest drag coefficient, the recirculation region is

reduced as shown in Figure 14 (b), but it seems not to be stable in Figure 15 (b). This fact may explain the increase in drag and the drag caused inside the conduit. The favorable configuration acts on the recirculation zone in a somewhat stable manner thanks to the decrease in dimensions in the exit.

In Figure 16, velocity contours within the central plane of the conduit are presented, illustrating both favorable and unfavorable scenarios. Uniform conduits have a greater impact on the recirculation region within the conduit's mid–plane compared to narrowed conduits. However, narrowed conduits exhibit more stability in their effect on the recirculation region.

Figure 17 and Figure 18 provide a comparative analysis of pressure coefficient contours for the specified configurations. While Figure 17 focuses on illustrating the pressure distribution on the symmetry plane, Figure 18 delves into depicting it along the body's rear.

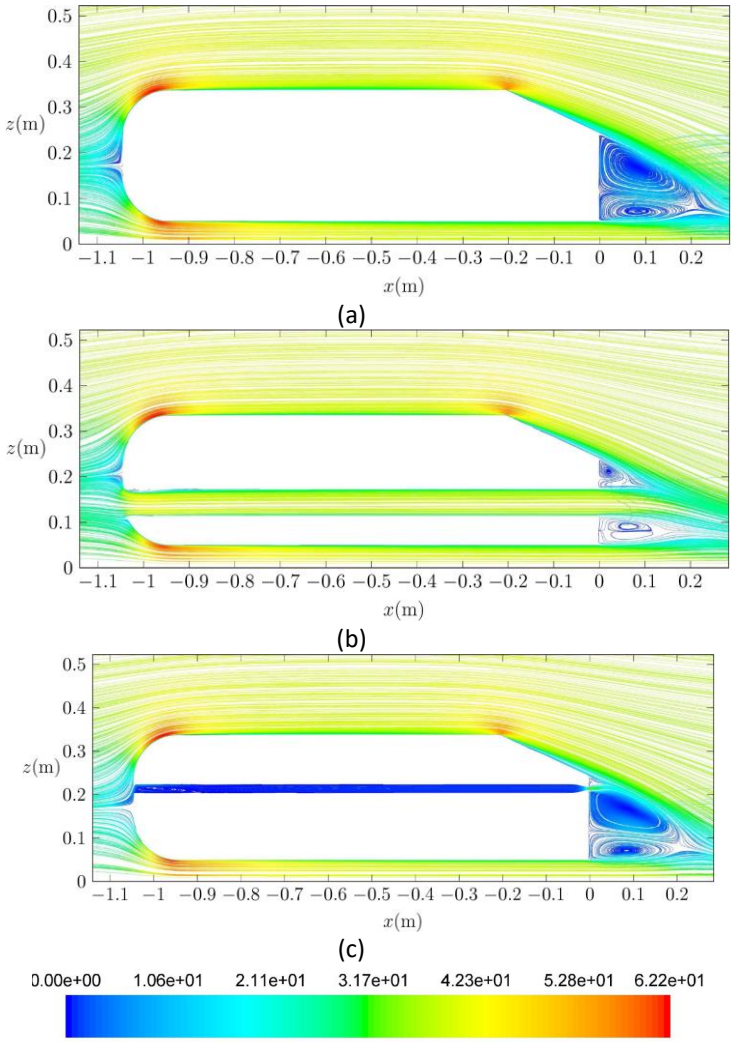

Fig. 14. Streamlines at the plane of symmetry (m.s^{-1}) for the: (a) standard Ahmed body 25° slant angle (b) unfavorable conduit arrangement (c) preferred conduit arrangement

The pressure coefficient on the body surface remains almost uniform. This can be attributed to the conduit being perforated into the body, causing the pressure to act internally. In cases of uniform conduits, such as depicted in Figure 17 (b), the internal pressure stays relatively stable compared to the external pressure. However, in situations where the conduit narrows at the exit, as seen in Figure 17 (c), the velocity inside the conduit decreases, resulting in an increase in pressure. As the

ratio *R* increases, there is a proportional increase in pressure within the conduits and a decrease in air velocity, potentially leading to a reduction in drag induced by the conduit.

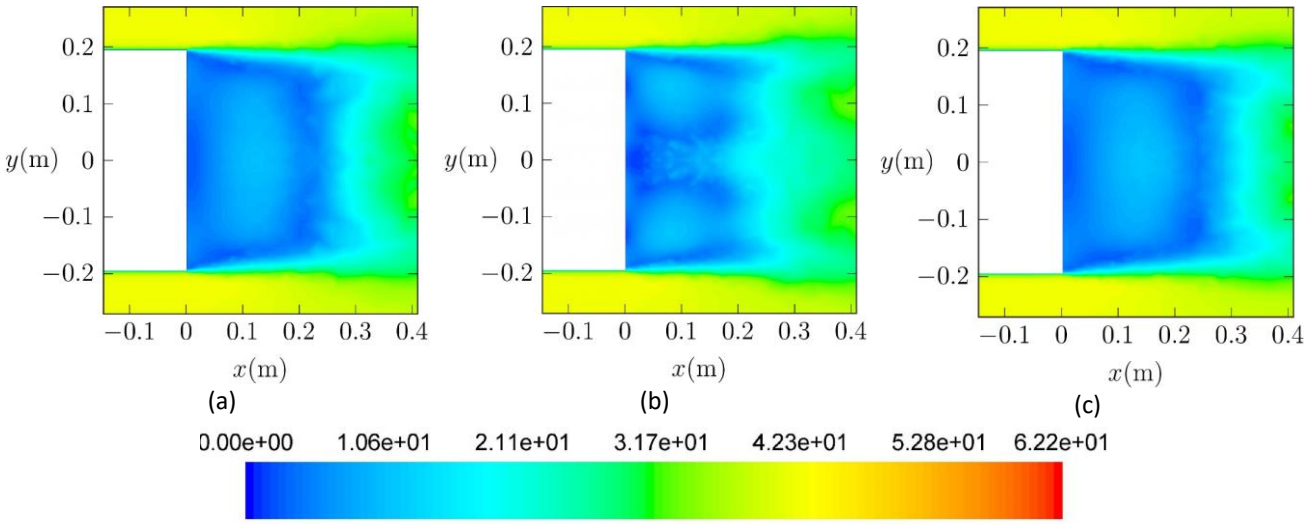

Fig. 15. Velocity contours (m.s^{-1}) at the plane *z* = 0.1 m for the (a) standard Ahmed body 25° slant angle (b) unfavorable conduit arrangement (c) preferred conduit arrangement

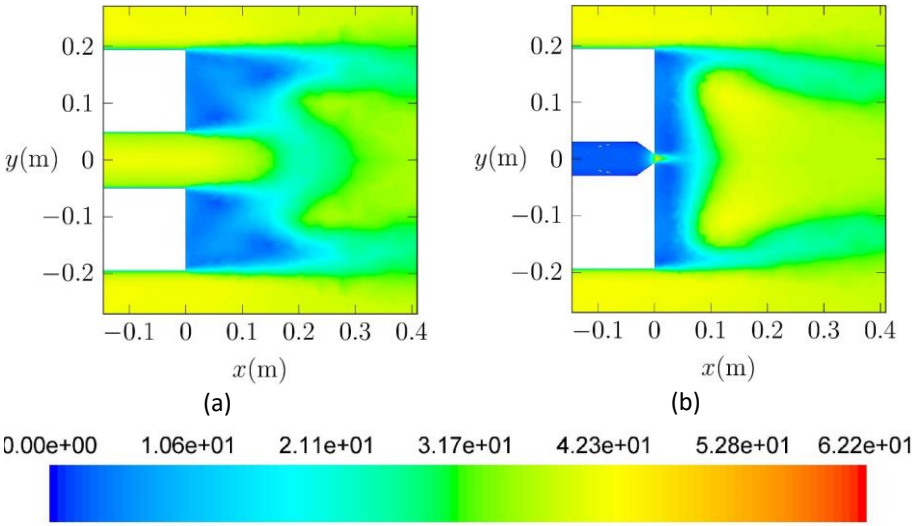

Fig. 16. Velocity contours (m.s^{-1}) at the conduit's central plane for the (a) unfavorable conduit arrangement (b) preferred conduit arrangement

For the Ahmed body, the base drag originates from the body's rear, constituting approximately 31.5% of the overall drag in our study. This aligns with findings from previous research, with Hanfeng *et al.,* [17] reporting 36% and Hung Tran *et al.,* [37] reporting 26%.

Regarding the use of the conduit within the body, the drag coefficient on the rear surface is minimally affected. In the unfavorable case, the portion of the rear end on the total drag is about 30%, while it remains the same for the convenient case. As a result, even though the conduit modifies the flow characteristics along the body, its impact on the rear end's drag contribution remains relatively limited. This suggests that the conduit's design and placement are optimized to enhance aerodynamic efficiency without significantly affecting drag at the rear end.

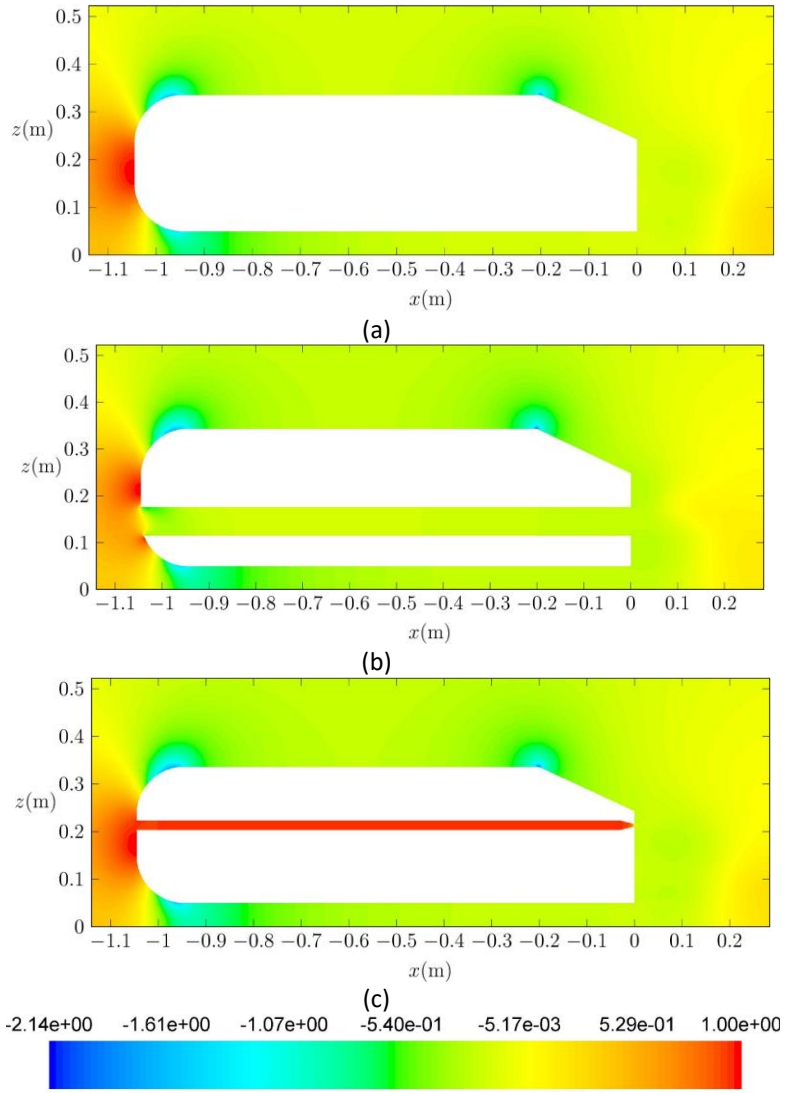

Fig. 17. Pressure coefficient contours at the symmetry plane for the (a) standard Ahmed body 25° slant angle (b) unfavorable conduit arrangement (c) preferred conduit arrangement

Figure 19, Figure 20 and Figure 21 represent contours illustrating turbulent kinetic energy (TKE) for specific configurations. TKE characterizes the turbulent flow stability. The significant turbulent kinetic energy implies that the flow downstream lacks stability.

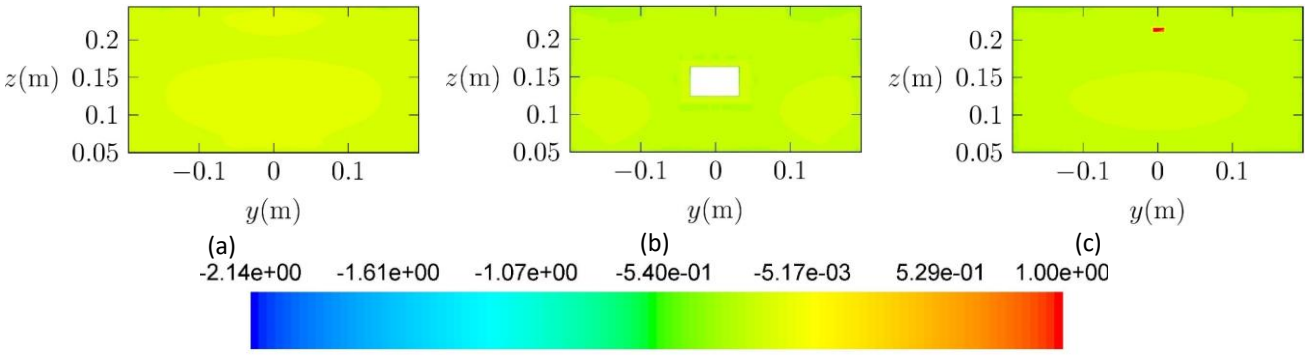

Fig. 18. Pressure coefficient contours at the body's rear for the (a) standard Ahmed body 25° slant angle (b) unfavorable conduit arrangement (c) preferred conduit arrangement

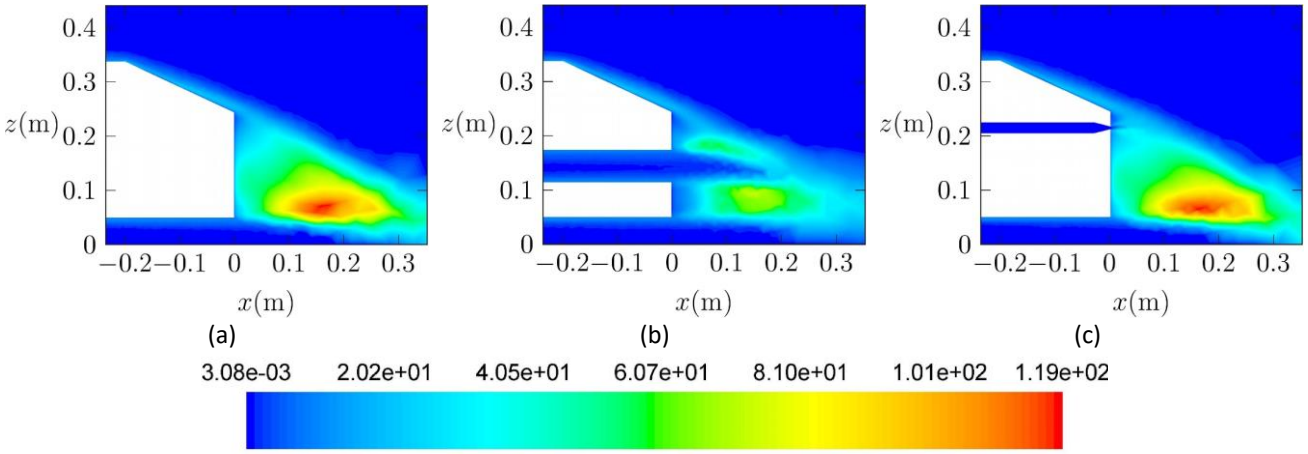

Fig. 19. Contours representation at symmetrical plane of TKE ($m^2.s^{-2}$) for the (a) standard Ahmed body 25° slant angle (b) unfavorable conduit arrangement (c) preferred conduit arrangement

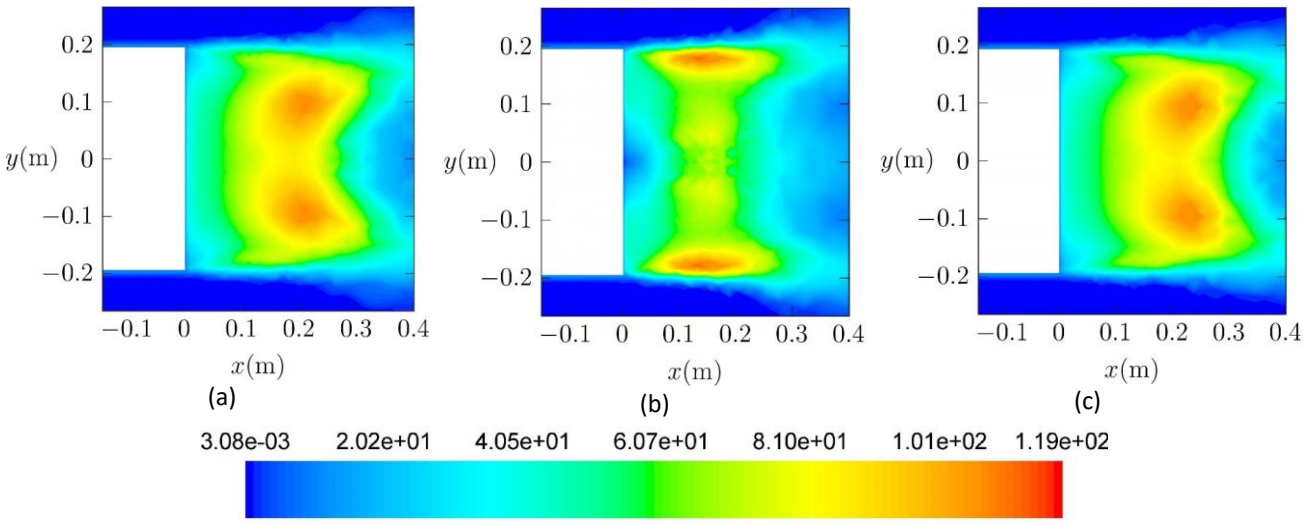

Fig. 20. Contours representation of TKE ($m^2.s^{-2}$) at the plane z = 0.1 m for the (a) standard Ahmed body 25° slant angle (b) unfavorable conduit arrangement (c) preferred conduit arrangement

In examining Figure 19, it becomes apparent that the contours of turbulent kinetic energy (TKE) in the unfavorable case (Figure 19 (b)) show a reduction in its shape, within the symmetry plane. Conversely, in Figure 20, the TKE contours in the unfavorable case (Figure 20 (b)) demonstrate a noticeable increase, at the z = 0.1 m plane. The observed decrease in TKE contours in Figure 19 (b) and the increase in Figure 20 (b) suggest variations in turbulence levels within the flow. These changes in TKE contours indicate altered turbulence characteristics, potentially influencing flow stability and may increase drag. For the favorable configuration, the TKE is identical to that of the standard Ahmed body. This configuration does not affect the stability of the flow on Ahmed body. On the contrary, the conduit in this case acts on the recirculation zone without affecting the flow stability.

Figure 21 confirms that while uniform conduits affect the recirculation region, turbulence levels in the conduit's mid–plane are higher compared to narrowed conduits.

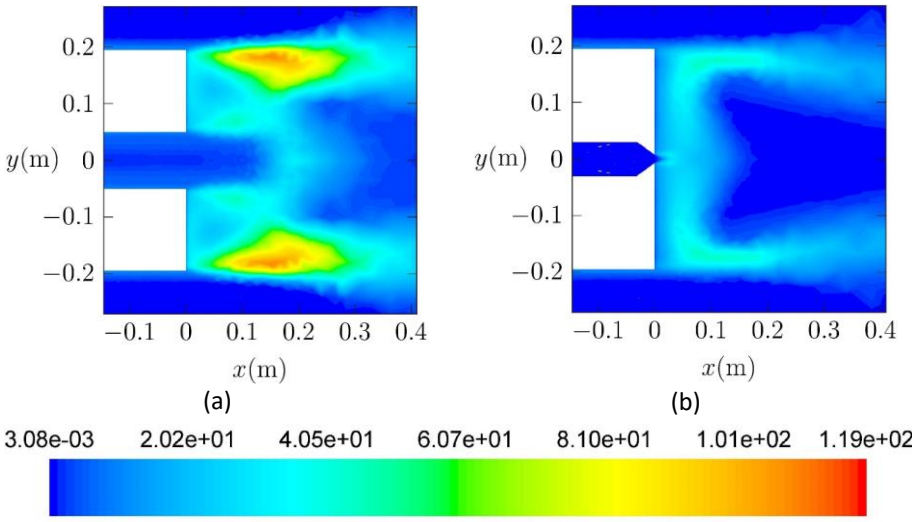

Fig. 21. Contours representation of TKE ($m^2.s^{-2}$) at the conduit's central plane for the (a) unfavorable conduit arrangement (b) preferred conduit arrangement

When utilizing the conduit along the Ahmed body, the TKE decreases, indicating smoother airflow. Simultaneously, the recirculation region diminishes, suggesting improved flow control. However, the pressure on the rear end of the body remains unchanged, implying that the conduit's effect primarily influences flow dynamics rather than altering pressure distributions.

In conclusion, our study successfully identified the optimal configuration for drag reduction using a perforated conduit in the Ahmed body. However, it's essential to recognize the limitations inherent in our methodology, especially concerning the extent of our numerical simulations. To enhance the generalizability of our results across a wider range of scenarios, future research will undertake a more exhaustive exploration of varied conditions. In addition, this study focused solely on a single Reynolds number. To broaden our understanding, it's imperative to investigate the effects across different Reynolds numbers in future studies.

4. Conclusion

This research conducted numerical simulations on the Ahmed body with a slant angle of 25°, subjected to a flow velocity of 40 $m.s^{-1}$. The primary objective centered on the strategic implementation of a rectangular conduit within the body, redirecting airflow from the front to the body rear, where recirculation is observed.

The study involved examining different configurations of uniform and exit-narrowed conduits, positioned at various locations from the lower slant edge. It ultimately identified an optimal configuration with dimensions measuring 0.06 m in length and 0.02 m in width. Placed at 0.04 m from the lower slant edge, this setup incorporates an exit reduction with a ratio of 4, resulting in a significant 3% decrease in drag.

Future endeavors will focus on studying the conduit inclination at the exit. Subsequently, it is crucial to conduct experimental studies to validate this innovative technique. The practical application of this method in automotive vehicles is the essential perspective offering a tangible solution for drag reduction in real–world scenarios.

Acknowledgement
This research was not funded by any grant.

References

[1] Choi, Haecheon, Jungil Lee, and Hyungmin Park. "Aerodynamics of heavy vehicles." *Annual Review of Fluid Mechanics* 46, no. 1 (2014): 441-468. https://doi.org/10.1146/annurev-fluid-011212-140616.

[2] Ahmed, Syed R., G. Ramm, and Gunter Faltin. "Some salient features of the time-averaged ground vehicle wake." *SAE transactions* (1984): 473-503. https://doi.org/10.4271/840300.

[3] Meng, Xueguang, Chengjian Deng, Dingsheng Wang, and Shujie Jiang. "Numerical study on the aerodynamic performance of the three-dimensional wing of a jellyfish-like flyer." *Frontiers in Physics* 11 (2023): 1125205. https://www.frontiersin.org/articles/10.3389/fphy.2023.1125205.

[4] Agriss, Amine, Mohamed Agouzoul, Abdeslem Ettaouil, and Abdessamad Mehdari. "Numerical study of new techniques drag reduction: application to aerodynamic devices." *International Journal for Simulation and Multidisciplinary Design Optimization* 12 (2021): 16. https://doi.org/10.1051/smdo/2021015.

[5] Oruc, Vedat. "Strategies for the applications of flow control downstream of a bluff body." *Flow Measurement and Instrumentation* 53 (2017): 204-214. https://doi.org/10.1016/j.flowmeasinst.2016.08.008.

[6] Abbasi, Waqas Sarwar, Saba Ismail, Sumaira Nadeem, Hamid Rahman, Afraz Hussain Majeed, Ilyas Khan, and Abdullah Mohamed. "Passive control of wake flow behind a square cylinder using a flat plate." *Frontiers in Physics* 11 (2023): 1132926. https://www.frontiersin.org/articles/10.3389/fphy.2023.1132926.

[7] Agriss, Amine, Mohamed Agouzoul, and Abdeslem Ettaouil. "Drag Reduction of a NACA Aerodynamic Airfoil: A Numerical Study." *Journal of Fluid Flow* 10 (2023). https://doi.org/10.11159/jffhmt.2023.013.

[8] Abdolahipour, Soheila. "Effects of low and high frequency actuation on aerodynamic performance of a supercritical airfoil." *Frontiers in Mechanical Engineering* 9 (2023): 1290074.

[9] Ngaongam, Choosak, and Rapee Ujjin. "Aerodynamic Characteristics of Forward Swept Wing in Subsonic Speed." *CFD Letters* 16, no. 5 (2024): 1-8. https://doi.org/10.37934/cfdl.16.5.18.

[10] Abidin, Harris Fadzillah Zainal, Md Tasyrif Abdul Rahman, Abdul Hamid Adom, Mohd Ridzuan Mohd Jamir, Sufi Suraya Halim, and Mohd Al Hafiz Mohd Nawi. "An Analysis of Urban Vehicle Body Aerodynamics Using Computational Fluid Dynamics for the Shell Eco-Marathon Challenge." *Journal of Advanced Research in Applied Sciences and Engineering Technology* 30, no. 2 (2023): 75-91. https://doi.org/10.37934/araset.30.2.7591.

[11] Howell, Jeff, David Sims-Williams, Adam Sprot, Fred Hamlin, and Robert Dominy. "Bluff body drag reduction with ventilated base cavities." *SAE International Journal of Passenger Cars-Mechanical Systems* 5, no. 1 (2012). https://doi.org/10.4271/2012-01-0171.

[12] Gilliéron, Patrick, and Azeddine Kourta. "Aerodynamic drag reduction by vertical splitter plates." *Experiments in fluids* 48, no. 1 (2010): 1-16. https://doi.org/10.1007/s00348-009-0705-7.

[13] Thacker, Adrien, S. Aubrun, A. Leroy, and Philippe Devinant. "Effects of suppressing the 3D separation on the rear slant on the flow structures around an Ahmed body." *Journal of Wind Engineering and Industrial Aerodynamics* 107 (2012): 237-243. https://doi.org/10.1016/j.jweia.2012.04.022.

[14] Kim, Dongri, Hoon Lee, Wook Yi, and Haecheon Choi. "A bio-inspired device for drag reduction on a three-dimensional model vehicle." *Bioinspiration & biomimetics* 11, no. 2 (2016): 026004. https://doi.org/10.1088/1748-3190/11/2/026004.

[15] Tian, Jie, Yingchao Zhang, Hui Zhu, and Hongwei Xiao. "Aerodynamic drag reduction and flow control of Ahmed body with flaps." *Advances in Mechanical Engineering* 9, no. 7 (2017): 1687814017711390. https://doi.org/10.1177/1687814017711390.

[16] Mohammadikalakoo, Babak, Paolo Schito, and Mahmoud Mani. "Passive flow control on Ahmed body by rear linking tunnels." *Journal of Wind Engineering and Industrial Aerodynamics* 205 (2020): 104330. https://doi.org/10.1016/j.jweia.2020.104330.

[17] Hanfeng, Wang, Zhou Yu, Zou Chao, and He Xuhui. "Aerodynamic drag reduction of an Ahmed body based on deflectors." *Journal of Wind Engineering and Industrial Aerodynamics* 148 (2016): 34-44. https://doi.org/10.1016/j.jweia.2015.11.004.

[18] Siddiqui, Naseeb Ahmed, and Martin Agelin-Chaab. "Investigation of the wake flow around the elliptical Ahmed body using detached Eddy simulation." *International Journal of Heat and Fluid Flow* 101 (2023): 109125. https://doi.org/10.1016/j.ijheatfluidflow.2023.109125.

[19] Aubrun, Sandrine, Jonathan McNally, Farrukh Alvi, and Azeddine Kourta. "Separation flow control on a generic ground vehicle using steady microjet arrays." *Experiments in fluids* 51 (2011): 1177-1187. https://doi.org/10.1007/s00348-011-1132-0.

[20] Wang, Bing-xin, Zhi-gang Yang, and Hui Zhu. "Active flow control on the 25 Ahmed body using a new unsteady jet." *International Journal of Heat and Fluid Flow* 79 (2019): 108459. https://doi.org/10.1016/j.ijheatfluidflow.2019.108459.

[21] Krentel, Daniel, Rifet Muminovic, André Brunn, Wolfgang Nitsche, and Rudibert King. "Application of active flow control on generic 3D car models." In *Active Flow Control II: Papers Contributed to the Conference" Active Flow Control II 2010", Berlin, Germany, May 26 to 28, 2010*, pp. 223-239. Berlin, Heidelberg: Springer Berlin Heidelberg, 2010. https://doi.org/10.1007/978-3-642-11735-0_15.

[22] Kourta, Azeddine, and Cédric Leclerc. "Characterization of synthetic jet actuation with application to Ahmed body wake." *Sensors and Actuators A: Physical* 192 (2013): 13-26. https://doi.org/10.1016/j.sna.2012.12.008.

[23] Wang, Bingxin, Zhigang Yang, and Hui Zhu. "Drag reduction on the 25◦ Ahmed body using a new zero-net-mass-flux flow control method." *Theoretical and Computational Fluid Dynamics* 33, no. 5 (2019): 411-431. https://doi.org/10.1007/s00162-019-00500-3.

[24] Brunn, Andre, Lars Henning, Wolfgang Nitsche, and Rudibert King. "Application of slope-seeking to a generic car model for active drag control." In *26th AIAA applied aerodynamics conference*, p. 6734. 2008. https://doi.org/10.2514/6.2008-6734.

[25] Bruneau, Charles-Henri, Emmanuel Creusé, Patrick Gilliéron, and Iraj Mortazavi. "Effect of the vortex dynamics on the drag coefficient of a square back Ahmed body: Application to the flow control." *European Journal of Mechanics-B/Fluids* 45 (2014): 1-11. https://doi.org/10.1016/j.euromechflu.2013.11.003.

[26] Plumejeau, Baptiste, Laurent Keirsbulck, Jérémy Basley, Marc Lippert, Sébastien Delprat, and Wafik Abassi. "Drag mitigation by steady blowing and Coanda effect on a square back Ahmed body." *European Journal of Mechanics-B/Fluids* 98 (2023): 80-91. https://doi.org/10.1016/j.euromechflu.2022.11.006.

[27] Wang, X. W., Y. Zhou, Y. F. Pin, and Tat Leung Chan. "Turbulent near wake of an Ahmed vehicle model." *Experiments in fluids* 54 (2013): 1-19. https://doi.org/10.1007/s00348-013-1490-x.

[28] Boussinesq, Joseph. "Theorie de l'ecoulement tourbillant." *Mem. Acad. Sci.* 23 (1877): 46.

[29] Menter, Florian R. "Two-equation eddy-viscosity turbulence models for engineering applications." *AIAA journal* 32, no. 8 (1994): 1598-1605. https://doi.org/10.2514/3.12149.

[30] E H (Ed.), Hirschel. Notes on Numerical Fluid Mechanics and Multidisciplinary Design. Vol. 82. Numerical Flow Simulation III. Springer, Berlin, Heidelberg, 2003.

[31] Inc. ANSYS. ANSYS Fluent Theory Guide, Release 17.0. Southpointe 2600 ANSYS Drive Canonsburg, PA 15317, 2016.

[32] Guilmineau, Emmanuel, G. B. Deng, Alban Leroyer, P. Queutey, Michel Visonneau, and J. Wackers. "Assessment of hybrid RANS-LES formulations for flow simulation around the Ahmed body." *Computers & Fluids* 176 (2018): 302-319. https://doi.org/10.1016/j.compfluid.2017.01.005.

[33] Thomas, Bryce, and Ramesh K. Agarwal. "Evaluation of various RANS turbulence models for predicting the drag on an Ahmed body." In *AIAA Aviation 2019 forum*, p. 2919. 2019. https://doi.org/10.2514/6.2019-2919.

[34] Fourrié, Grégoire, Laurent Keirsbulck, Larbi Labraga, and Patrick Gilliéron. "Bluff-body drag reduction using a deflector." *Experiments in Fluids* 50 (2011): 385-395. https://doi.org/10.1007/s00348-010-0937-6.

[35] Agriss, A., M. Agouzoul, A. Ettaouil, and A. Mehdari. "Numerical Investigation of a Drag Reduction Device Applied to the Ahmed Body." *International Review on Modelling and Simulations (IREMOS)* 15, no. 2. https://doi.org/10.15866/iremos.v15i2.22103.

[36] Guilmineau, Emmanuel. "Computational study of flow around a simplified car body." *Journal of wind engineering and industrial aerodynamics* 96, no. 6-7 (2008): 1207-1217. https://doi.org/10.1016/j.jweia.2007.06.041.

[37] Tran, The Hung, Masato Hijikuro, Masayuki Anyoji, Takanori Uchida, Takuji Nakashima, and Keigo Shimizu. "Surface flow and aerodynamic drag of Ahmed body with deflectors." *Experimental Thermal and Fluid Science* 145 (2023): 110887. https://doi.org/10.1016/j.expthermflusci.2023.110887.

[38] Rodriguez, Romain, Frédéric Murzyn, Amine Mehel, and Frederique Larrarte. "Dispersion of ultrafine particles in the wake of car models: A wind tunnel study." *Journal of Wind Engineering and Industrial Aerodynamics* 198 (2020): 104109. https://doi.org/10.1016/j.jweia.2020.104109..